Transparent Thermoelectric Device for Simultaneously Harvesting Radiative Cooling and Solar Heating

Satoshi Ishii,[1,2,*] Cédric Bourgès,[1,3] Nicholaus K. Tanjaya,[1,2] Takao Mori[1,2]

[1] Research Center for Materials Nanoarchitectonics (MANA), National Institute for Materials Science (NIMS), 1-1 Namiki, Tsukuba, Ibaraki 305-0044, Japan.

[2] Subprogram in Materials Science and Engineering, Graduate School of Science and Technology, University of Tsukuba, Tsukuba, Ibaraki 305-8577, Japan.

[3] International Center for Young Scientists, National Institute for Materials Science (NIMS), 1-1 Namiki, Tsukuba, 305-0044, Japan

*E-mail address: sishii@nims.go.jp

Keywords: radiative cooling, solar heating, thermoelectric generator, energy harvesting, thermal radiation

Abstract

Outdoor radiative cooling is a passive method of cooling a surface that faces the sky. During the past decade, numbers of successful demonstrations of daytime radiative coolers have been reported. Because a daytime radiative cooler can be radiatively cooled both during the day and at night, it is always cooled and a temperature difference against the surroundings is generated. This temperature difference can be used to generate thermoelectric power throughout the day by placing a daytime radiative cooler on a thermoelectric module. However, such a device cannot harvest solar heat because sunlight is reflected by the daytime radiative cooler. In this study, a thermoelectric device that simultaneously harvests both radiative cooling and solar heating is presented. The essential component is a vertically placed thermoelectric module made of transparent thermoelectric thin films which allows radiatively cooled and solar heated surfaces to be co-planar. The outdoor and indoor measurements confirm that the device can harvest both radiative cooling and solar heating simultaneously during the day without offsetting each other, and can harvest radiative cooling at night. The co-planar design is an efficient method for simultaneously harvesting solar heating and radiative cooling, which could facilitate efficient energy harvesting and can be applied to a standalone power supply for off-grid sensor modules.

Introduction

Outdoor radiative cooling is a passive method of cooling surfaces facing the sky. While nighttime radiative cooling occurs whenever the sky is clear, daytime radiative cooling is unconventional. However, initiated by early works in the 70s and 80s [1,2] several successful demonstrations of daytime radiative cooling have been reported. High solar reflectance and high emissivity in the mid-infrared (MIR) region are essential for achieving daytime radiative cooling.[3-7] Various materials and types of structures have been investigated, including organics,[8-12] inorganics,[13-17] and natural materials,[18] which include multilayers,[13-17] porous structures,[8,10,19-21] and particle dispersion in polymers.[22-25]

Well-designed daytime radiative coolers can cool to sub-ambient temperatures without electricity, which is crucial in modern society that faces global warming. Notably, temperature difference exists when the radiative cooler is at a sub-ambient temperature. Because a daytime radiative cooler is radiatively cooled both during the day and at night, temperature differences can be generated throughout the day.

To utilize the temperature difference caused by radiative cooling for harvesting energy, thermoelectric modules [26] can be placed below thermal emitters to thermally conducted temperature differences. Initial studies used blackbody coatings as thermal emitters that were radiatively cooled only at night.[27-34] As a blackbody has high solar absorptance, it is heated during day and generates a thermoelectric voltage with the opposite sign compared to that generated at night. Although such devices can generate thermoelectric power in day and night, the voltage drops to zero when day/night turns to night/day and by sudden weather changes, such as the appearance of a cloud.

Daytime radiative coolers combined with thermoelectric modules have demonstrated thermoelectric power generation throughout the day without the voltage dropping to zero.[35-39] Compared with a device containing a blackbody thermal emitter on a thermoelectric module, a device containing a daytime radiative cooler on a thermoelectric module provides a more stable output throughout the day without sign changes in the thermoelectric voltage. However, as long as sunlight is reflected by the daytime radiative cooler, solar energy does not contribute to thermoelectric generation, which is wasted.

Recently, novel designs that can simultaneously harvest solar heat and radiative cooling have been developed.[12,40-44] Within a device, there were solar absorbing and radiative cooling regions such that a temperature difference was generated by solar heating and radiative cooling during the day. Consequently, the temperature differences were larger than those obtained using radiative cooling only. Nevertheless, all the designs had separate solar absorbing and radiative cooling regions; therefore, the device areas were not being used efficiently during the day. To maximize outdoor energy harvesting per unit area, it is desirable to make solar heated and radiatively cooled surfaces to be co-planar and place a transparent thermoelectric module between them. The transparency of thermoelectric module is crucial to generate solar heat at the bottom surface without blocking sunlight. In an early attempt to demonstrate the concept, a

solar-transparent magnetic material was chosen and the spin Seebeck effect, which is a spintronic version of Seebeck effect, was utilized for thermoelectric generation.[45] The fabricated device harvested solar heat and radiative cooling simultaneously in the same plane; however, the outdoor output voltage was of the order of sub-microvolts owing to the small out-of-plane temperature gradient and extremely low efficiency of the spin Seebeck effect.

In the current study, we address these problems using transparent thermoelectric materials. Transparent thermoelectric materials have been investigated, which include zinc oxide,[46] aluminum-doped zinc oxide,[47] indium tin oxide,[48] and IGZO [49,50] as *n*-type materials, and copper iodide (CuI) as a *p*-type material [51-54]. Additionally, transparent thermoelectric modules have been demonstrated; however, thus far, these modules considered temperature differences parallel to the substrates that were transparent.[53,55,56] Unlike previous studies, the proposed design in this work had *n*- and *p*-type transparent films deposited on each side of a transparent substrate to form a *p*-*n* junction that was placed perpendicular to the bottom solar absorber and top transparent radiative cooler. This design ensured that the in-plane temperature difference was of the order of unity by the solar heating and radiative cooling, and the simultaneous harvesting of solar heat and radiative cooling was achieved with the co-planar geometry. The transparent thermoelectric materials used in this study were IZGO and CuI, and indoor experiments proved that the device could simultaneously harvest solar heating and radiative cooling without interference. Outdoor experiments demonstrated that the device could generate thermoelectric voltage without sign changes, throughout the day. In addition, several strategies to improve the output have been proposed, supported by the experimental demonstrations.

Results and discussion

Figure 1(a) shows a schematic of the device. The thermoelectric generator, which was located at the center, consisted of *p*- and *n*-type transparent thermoelectric thin films sandwiched between a solar-transparent and MIR-opaque plate at the top and blackbody-paint-coated plate at the bottom. Because the top plate and thermoelectric generator are transparent to sunlight, the bottom plate is always irradiated with sunlight during the day, regardless of the solar irradiation angle, as illustrated in Figure 1(b). As the top plate is sunlight-transparent and MIR-opaque, it thermally radiates to the sky during the day and night. Thus, on the same day, a temperature difference is generated to the thermoelectric generator by solar heating at the bottom and radiative cooling at the top. At night, the temperature difference is caused only by radiative cooling at the top.

The transparent thermoelectric films that are perpendicular to the bottom and top plates are unique features of the device. Assuming a solar irradiance of 1000 W/m^2 and thermal radiation to the sky, the estimated temperature difference between the top and bottom of the thermoelectric generator was 4.66 K as shown in Figure 1(c). This perpendicular geometry

strongly contrasts with the parallel geometry, in which thermoelectric films are deposited on a bottom plate (Figure S1(a)). The parallel geometry also facilitates the simultaneous harvesting of solar heat and radiative cooling during the day; however, the temperature difference is along the thickness direction of the thermoelectric films. Because the visible transparency of thermoelectric films decreases with increasing thickness, the thickness should be less than 1000 nm to maintain visible transparency (Figure S1(b)). As shown in Figure S1(c), the estimated temperature difference in the parallel design, which was obtained by solar heating and radiative cooling, was of sub-millikelvin order along the thickness direction of a few hundred nanometers. A temperature difference of more than three orders of magnitude between the perpendicular and parallel geometries highlights the advantages of the perpendicular geometry.

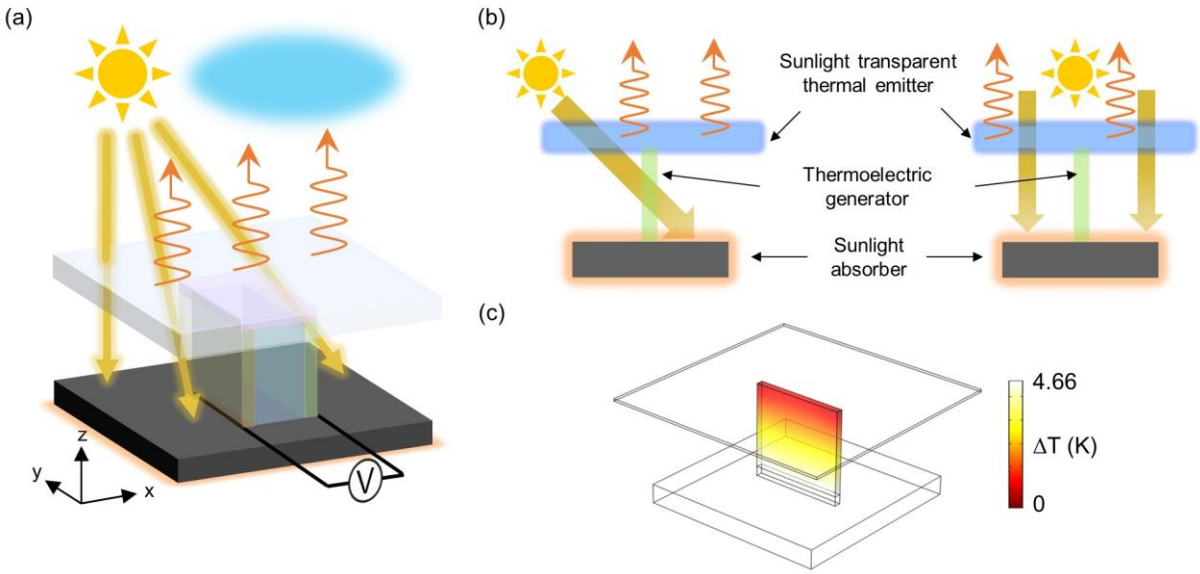

Figure 1. (a) Schematic of the device. A transparent thermoelectric module is vertically placed between the top and bottom plates. The top plate is solar-transparent and MIR-opaque such that radiative cooling is achieved outdoors. The bottom plate is coated with blackbody paint such that it absorbs sunlight that is transmitted by the top panel. (b) Cross sectional view of the device illustrating oblique solar irradiance. Even at oblique incidence, sunlight irradiates the bottom plate as the thermoelectric module is transparent. (c) Numerically simulated temperature of the device by setting the solar irradiance and sky temperature as 1000 W/m^2 and 273 K, respectively.

To realize the transparent thermoelectric generator, IGZO and CuI were chosen as the *n*- and *p*-type thermoelectric materials, respectively. The X-ray diffraction (XRD) patterns of the IGZO and CuI films (Figure S2) indicate that the films were amorphous and polycrystalline, respectively. The thermoelectric properties of the two films are summarized in Table S1. IGZO (thickness: 150 nm) and CuI (thickness: 216 nm) thin films were fabricated on each side of the glass substrate. As shown in the optical image and transmittance spectrum in Figure 2(a), the

IGZO/glass/CuI sample exhibits high transparency in the solar spectrum. After forming the IGZO/glass/CuI, the IGZO and CuI thin films were electrically connected by a thin aluminum (Al) foil at the edge. The transparent thermoelectric generator was vertically attached to a bottom acrylic plate coated with blackbody paint, and a polyethylene terephthalate (PET) plate was attached to the top, as shown in Figure 2(b). The blackbody-paint-coated acrylic and PET plates acted as solar absorber and sunlight-transparent thermal radiators, respectively. The optical spectra and SEM images of the blackbody paint and PET plate are shown in Figure S3. Indoor experiments were performed to characterize the generation of thermoelectric voltages by radiative cooling and solar heating. Here, the blackbody-paint-coated Peltier module maintained at 0 °C and solar simulator at 333 W/m^2 mimicked the sky and sun, respectively. The voltages obtained by radiative cooling, solar heating, and their combination are summarized in Figure 2(c). The voltage of 0.68 mV with radiative cooling and solar heating is nearly equal to the sum of the voltages with radiative cooling (0.4 mV) and solar heating (0.28 mV). This suggests that the device can simultaneously harvest radiative cooling and solar heating. The Seebeck coefficients of IGZO and CuI (Table S1) were used to experimentally estimate the temperature difference within the device. For simultaneous radiative cooling and solar heating, the estimated temperature difference was 1.0 K. The temperature difference estimated by the numerical heat transfer simulations was 0.91 K, which is consistent with the experimental results.

The influence of the radiative heat transfer on the device was evaluated by changing the Peltier module temperature from 0 °C to 60 °C as shown in Figure 2(d). For these measurements, the solar simulator was switched off. As the temperature of the Peltier module increases from 0 °C, the voltage decreases and changes its sign when the temperature exceeds 30 °C, which is slightly above the room temperature. This sign change is reasonable; when the Peltier module is cooler/warmer than the room temperature, the device is cooled/heated by radiative heat transfer such that the temperature difference between the top and bottom of the device changes. Radiative heat transfer measurements using only the Peltier module were also conducted in vacuum by evacuating the chamber. The temperature dependence of the Peltier module in vacuum is shown in Figure S4. A higher voltage was recorded in vacuum than under ambient conditions, as shown in Figure 2(d) owing to the suppression of convective heat transfer. Although placing a device in vacuum effectively increases the voltage, maintaining it in vacuum is practically challenging.

In all the indoor measurements, the distance between the device and Peltier module was maintained at 110 mm to allow solar irradiation from the side. Thus, the geometric factor of the device and Peltier module was approximately 0.017, which indicated an inefficient radiative transfer. To study the effect of distance on the voltage, a set of separate measurements was performed at various distances under ambient conditions only using the Peltier module at 0 °C

and the results are plotted in Figure S5. The voltage increases with decreasing distance, which qualitatively corresponds to an increase in the geometrical factor.

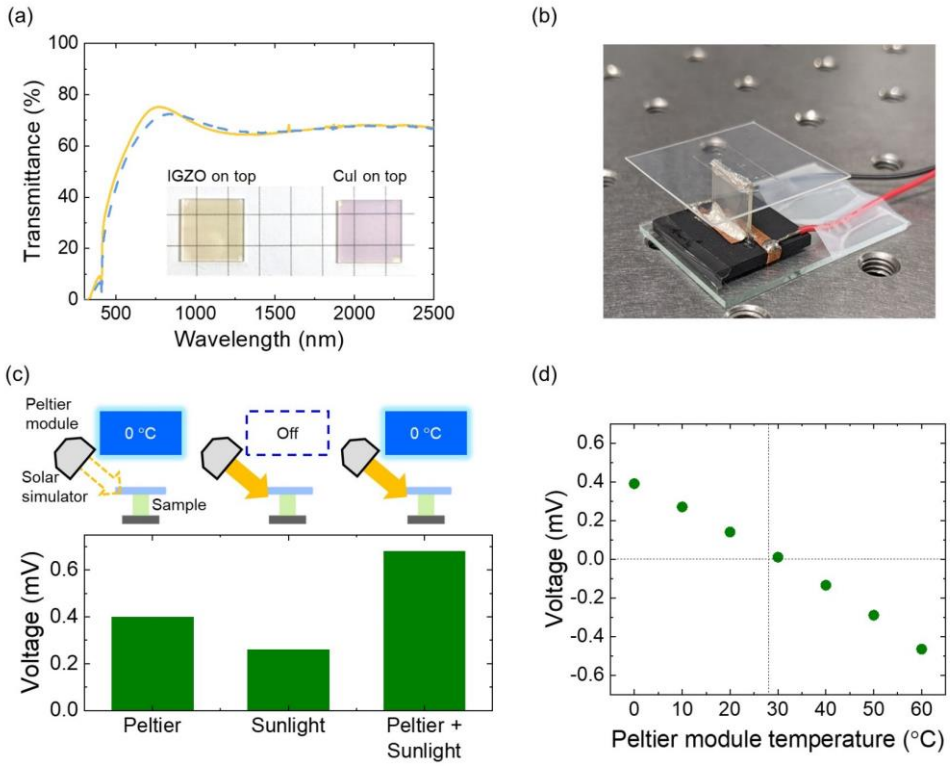

Figure 2. (a) Transmittance of IGZO/glass/CuI measured from the IGZO and CuI sides. The inset shows the photographs of IGZO/glass/CuI taken where the IGZO (left) and CuI (right) sides are facing up. (b) Photograph of the device. (c) Voltage measured indoors with only the Peltier module, only the solar simulator, and both the Peltier module and solar simulator. In each measurement, the Peltier module was set at 0 °C, while the solar irradiance was 333 W/m^2. (d) Peltier module temperature dependance of voltage where the Peltier module temperature ranged from 0 °C to 60 °C.

After confirming the performances in indoors, outdoor measurements were conducted on the roof of a five-floor building at the National Institute for Materials Science in Tsukuba, Ibaraki, Japan on August 3rd and 4th, 2022. The photograph and schematic of the setup are shown in Figures 3(a) and 3(b), respectively, where the device was covered with a thin transparent film to block wind. The measured voltage, outdoor temperature, and solar irradiance are plotted in Figures 3(c), 3(d) (left axis), and 3(d) (right axis), respectively. Figure 3(c) shows that continuous voltage generation is recorded for 24 hours. Because both solar heating and radiative cooling can be used to generate temperature differences in the device, the voltage was higher

during the day than at night. At night, only radiative cooling, which was considerably weaker than solar irradiance, generated temperature differences.

In the outdoor measurements presented in Figure 3, the heat from the roof was suppressed by a 30-mm thick polystyrene foam covered with Al foil, as illustrated in Figure 3(b). The measurement was also performed without the foam, as shown in Figures S6(a) and S6(b). Because the roof was warmer than the ambient temperature, the bottom of the device was heated from the roof in addition to solar heat. Therefore, the voltage shown in Figure S6(c) is higher than that shown in Figure 3(c) under similar weather conditions (Figures 3(b) and S6(d)).

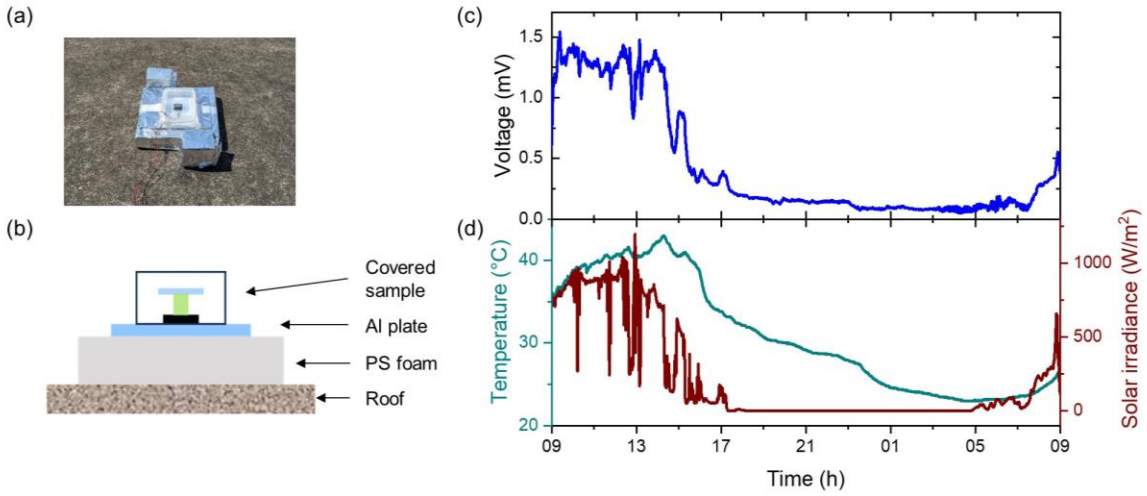

Figure 3. (a) Photograph and (b) schematic of the outdoor measurement setup which was placed on the roof of a five-floor building in Tsukuba, Japan from August 3rd to 4th 2022. The device was covered with a thin transparent film for windbreak. The 30-mm thick polystyrene (PS) foam suppressed the heat conduction and the 5-mm thick Al plate was used as a weight. Both PS foam and Al plate were covered with Al foil to reflect sunlight. (c) Voltage of the device and (d) ambient temperature and solar irradiance measured outdoors.

Thus far, the device studied had a height of approximately 10 mm and only one *p*-*n* junction. The voltage can be improved in a straightforward manner by increasing the device height and number of *p*-*n* junctions. The two strategies were tested individually. Figure 4(a) shows a photo of the three devices using glass substrates with widths of 10 mm, 15 mm, and 20 mm. Figure 4(b) shows the height dependence of the simulated temperature difference between the top and bottom of the device. The temperature difference increases with the height; however, the rate of increase decreases because the solar irradiance and radiative cooling are fixed. The numerically simulated height-dependent temperature difference was compared with the indoor experiments that measured the voltage. The indoor measurements were performed using a solar simulator and Peltier module to imitate solar irradiation and radiative cooling. As expected, similar height dependence was observed.

Figure 4(c) shows a photograph of the double *p-n* junction device. Its voltage was compared to that of a single *p-n* junction device in an indoor experiment with a Peltier module and solar simulator, as shown in Figure 4(d). The voltage nearly doubles when the number of *p-n* junctions increases from one to two. A further increase is expected by increasing the number of *p-n* junctions.

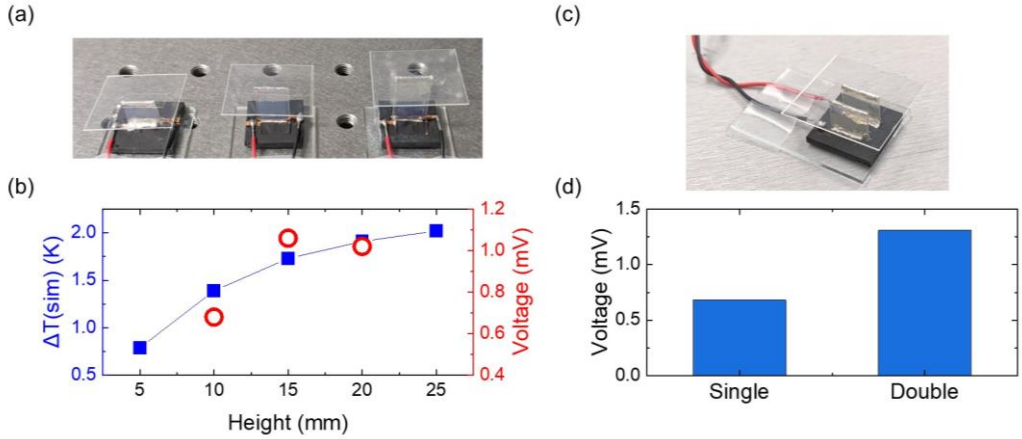

Figure 4. (a) Photograph of three devices where the widths of the glass substrates are 10 mm, 15 mm, and 20 mm. (b) Height dependence of the temperature difference (ΔT) and voltage. ΔT was obtained from numerical simulations based on the finite element method while the voltage was measured indoors. The value at a height of 10 mm is identical to that presented in Figure 2(c). (c) Photo of the device with double *p-n* junctions. (d) Voltage of devices containing single and double *p-n* junctions. The value for the single *p-n* junction is identical to that presented in Figure 2(c).

The results presented thus far have shown that the thermoelectric devices made of transparent materials can simultaneously harvest radiative cooling and solar heating if placed between a top solar-transparent plate and a bottom black plate. Even with a single *p-n* junction device, the outdoor measurement showed a millivolt output voltage during the day. The thermoelectric performance of the device outperforms other thermoelectric devices[12,40,41,45] that can harvest both radiative cooling and solar heat as shown in Table S2. Even though the other devices used Bi-Te based materials that have far better thermoelectric performances than IGZO and CuI, the vertical design maximized temperature difference to exhibit higher performance than others. The results presented in Figure 4 demonstrate the potential of further increasing the voltage. To increase the number of *p-n* junctions, in addition to adding more substrates with IGZO and CuI thin films on each side, fabricating multiple *p-n* junctions by patterning thin films can further increase the density of the *p-n* junctions. Referring to ref. [56], it is possible to fabricate 25 *p-n* junctions on 10-mm wide substrates. In addition to increasing the voltage, mechanical strength of the device must be improved; this aspect was not considered in the present study. Instead of covering the device with a transparent film, the top transparent plate

can also be designed as a shield that provides the entire device with better durability and mechanical strength. More outdoor field tests in different weathers and seasons are also necessary to investigate the device potential as an outdoor standalone power supply.

Conclusion

In summary, a thermoelectric device powered by harvesting solar heat and radiative cooling was proposed, and its power generation was demonstrated through outdoor and indoor experiments. While the transparent top plate of the device transmitted sunlight and thermally radiated to the sky, the bottom black plate absorbed sunlight to generate heat. The thermoelectric module was composed of IGZO and CuI thin films placed perpendicular between the top and bottom plates. Because the thin films and substrates were both transparent, the thermoelectric module did not block sunlight, regardless of the incident angles. At night, the device generated thermoelectric voltage via radiative cooling only. The device generated a thermoelectric voltage above 1 mV even with a single *p-n* junction. The ability of the device to continuously generate thermoelectric voltage during the day and night make it an ideal power supply for off-grid sensors that have been steadily increasing in recent years.

Sample fabrication

The IGZO thin film was deposited on a borosilicate glass by DC sputtering (!-Miller, Shibaura Mechatronics Co.) at 200 W using an IGZO target (Kojundo Chemical Lab. Co., Ltd.) under flows of argon and oxygen. The deposition was done without substrate heating and the deposition rate was 0.17 nm/s. To fabricate the CuI thin film, a Cu film was first deposited on a borosilicate glass using an electron-beam evaporator. The Cu film was iodized by placing it in a closed container with iodine beads for more than an hour at room temperature. Owing to the iodization, the CuI thickness increased nearly five times compared to the original Cu film.
To fabricate a device, the IGZO and CuI thin films were deposited on each side of a borosilicate glass substrate (10×10×t0.7 mm). Then, an Al foil was attached to electrically connect IGZO and CuI films to form a transparent thermoelectric generator. An acrylic plate (18×18×t2 mm) coated with blackbody paint (TA410KS, ICHINEN TASCO CO., LTD.) and a PET plate (25×25×t0.25 mm, Lumirror T60, Industries, Inc.) were attached to the bottom and top sides of the vertically placed thermoelectric generator.

Characterization

The UV-visible-NIR and MIR transmittances were measured using a UV-VIS spectrometer (V-770, JASCO) and Fourier-transform infrared spectroscopy (Nicolet iS50R FT-IR, Thermo Fisher Scientific K.K.), respectively.
The Seebeck coefficients and resistivities of the IGZO and CuI films were measured using a ZEM-3 (Ulvac, Co. Ltd.) at room temperature.

XRD patterns were measured using a thin-film X-ray diffractometer (X'Pert MRD, PANalytical Ltd.).

Indoor measurement

A Peltier module (LVPU-40, VICS Co., Ltd.) with a cooling and heating area of 70-mm square was coated with blackbody paint (TA410KS, ICHINEN TASCO CO., LTD.) and attached on top of the transparent acrylic chamber by facing the surface downward. The distance between the Peltier module surface and sample stage was approximately 110 mm, unless specified otherwise. A solar simulator (PEC-L01, Peccell Technologies, Inc.) was used to irradiate the samples from the sidewalls of the transparent acrylic chamber. Thus, while the radiative heat transfer occurred in the vertical direction, the solar simulator obliquely irradiated the sample. The surface temperature of Peltier module was tunable from 0 ℃ to 60 ℃ but it was maintained at 0 ℃ unless otherwise mentioned. Because of the oblique irradiation of the solar simulator, the average irradiance at the bottom of the sample could not reach the standard value of 1000 W/m^2 and was maintained at 333 W/m^2. Depending on the measurement, either the Peltier module, or solar simulator, or both, were turned on after placing the device inside the chamber. Under each condition, the voltage was recorded after thermal equilibrium was reached. The measurements were performed in a vacuum only when mentioned; otherwise, they were performed at ambient pressure in a closed chamber.

Outdoor measurement

The sample was placed on the roof of a five-floor building at the National Institute of Materials Science (36°04'07.8"N, 140°07'58.7"E) where it was shielded with a thin polyvinylidene chloride sheet to avoid convection. Temperature and humidity were recorded using a logger placed in a white instrument shelter. Solar irradiance was measured using a pyranometer.

Numerical calculations

In the heat transfer simulation, the heat transfer at the sample was modeled including the terms for solar absorptance, atmospheric radiation, and thermal radiation from the sample, and non-radiative terms, including conduction and convection.

Author contributions

S.I. and T.M. conceived the idea of the device. S.I. and N.T. fabricated the thin films, and S.I. fabricated the devices. S.I, C.B., and N.T. characterized the samples. S.I. performed indoor and outdoor measurements to characterize the voltage. All the authors were involved in the discussion and writing of the manuscript.

Corresponding Author

E-mail: sishii@nims.go.jp

ORCID

Satoshi Ishii: 0000-0003-0731-8428
Cédric Bourgès: 0000-0001-9056-0420
Nicholaus Tanjaya: 0000-0003-4126-8540
Takao Mori: 0000-0003-2682-1846

Competing interests

The authors declare no competing interests.

Acknowledgment

The authors thank E. Shimada for her assistance in the measurements. S.I. acknowledges the support from JST PRESTO (JPMJPR19I2), JST FOREST (JPMJFR2139) and Kakenhi from JSPS (22H01917), Japan. T.M. and C.B. thank JST Mirai Program JPMJMI19A1 for support.

Additional information

Supplementary information is available online.

References

[1] S. Catalanotti, V. Cuomo, G. Piro, D. Ruggi, V. Silvestrini, G. Troise, *Sol. Energy* **17** (2) (1975) 83.
[2] C. G. Granqvist, and A. Hjortsberg, *J. Appl. Phys.* **52** (6) (1981) 4205.
[3] M. Zeyghami, D. Y. Goswami, E. Stefanakos, *Sol. Energy Mater Sol. Cells* **178** (2018) 115.
[4] B. Zhao, M. Hu, X. Ao, N. Chen, G. Pei, *Appl. Energy* **236** (2019) 489.
[5] D. Zhao, A. Aili, Y. Zhai, S. Xu, G. Tan, X. Yin, R. Yang, *Appl. Phys. Rev.* **6** (2) (2019)
[6] M. Chen, D. Pang, X. Chen, H. Yan, Y. Yang, *EcoMat* **4** (1) (2022) e12153.
[7] S. Fan, and W. Li, *Nat. Photon.* **16** (3) (2022) 182.
[8] A. Leroy, B. Bhatia, C. C. Kelsall, A. Castillejo-Cuberos, M. Di Capua H., L. Zhao, L. Zhang, A. M. Guzman, E. N. Wang, *Sci. Adv.* **5** (10) (2019) eaat9480.
[9] S. Y. Jeong, C. Y. Tso, Y. M. Wong, C. Y. H. Chao, B. Huang, *Sol. Energy Mater Sol. Cells* **206** (2020) 110296.
[10] H. Zhong, Y. Li, P. Zhang, S. Gao, B. Liu, Y. Wang, T. Meng, Y. Zhou, H. Hou, C. Xue, Y. Zhao, Z. Wang, *ACS Nano* **15** (6) (2021) 10076.
[11] J. Li, X. Wang, D. Liang, N. Xu, B. Zhu, W. Li, P. Yao, Y. Jiang, X. Min, Z. Huang, S. Zhu, S. Fan, J. Zhu, *Sci. Adv.* **8** (32) (2022) eabq0411.
[12] W. B. Han, S.-Y. Heo, D. Kim, S. M. Yang, G.-J. Ko, G. J. Lee, D.-J. Kim, K. Rajaram,

J. H. Lee, J.-W. Shin, T.-M. Jang, S. Han, H. Kang, J. H. Lim, D. H. Kim, S. H. Kim, Y. M. Song, S.-W. Hwang, *Sci. Adv.* **9** (5) (2023) eadf5883.
[13] A. P. Raman, M. A. Anoma, L. Zhu, E. Rephaeli, S. Fan, *Nature* **515** (7528) (2014) 540.
[14] J.-L. Kou, Z. Jurado, Z. Chen, S. Fan, A. J. Minnich, *ACS Photonics* **4** (3) (2017) 626.
[15] D. Chae, M. Kim, P.-H. Jung, S. Son, J. Seo, Y. Liu, B. J. Lee, H. Lee, *ACS Appl. Mater. Interfaces* **12** (7) (2020) 8073.
[16] T. Suichi, A. Ishikawa, T. Tanaka, Y. Hayashi, K. Tsuruta, *Sci. Rep.* **10** (1) (2020) 6486.
[17] S. Ishii, D. Hernández-Pinilla, N. K. Tanjaya, T. Nagao, *Sol. Energy Mater Sol. Cells* **259** (2023) 112463.
[18] T. Li, Y. Zhai, S. He, W. Gan, Z. Wei, M. Heidarinejad, D. Dalgo, R. Mi, X. Zhao, J. Song, J. Dai, C. Chen, A. Aili, A. Vellore, A. Martini, R. Yang, J. Srebric, X. Yin, L. Hu, *Science* **364** (6442) (2019) 760.
[19] P.-C. Hsu, A. Y. Song, P. B. Catrysse, C. Liu, Y. Peng, J. Xie, S. Fan, Y. Cui, *Science* **353** (6303) (2016) 1019.
[20] Y. Fu, J. Yang, Y. S. Su, W. Du, Y. G. Ma, *Sol. Energy Mater Sol. Cells* **191** (2019) 50.
[21] D. Lee, M. Go, S. Son, M. Kim, T. Badloe, H. Lee, J. K. Kim, J. Rho, *Nano Energy* **79** (2021) 105426.
[22] Y. Zhai, Y. Ma, S. N. David, D. Zhao, R. Lou, G. Tan, R. Yang, X. Yin, *Science* **355** (6329) (2017) 1062.
[23] X. Li, J. Peoples, Z. Huang, Z. Zhao, J. Qiu, X. Ruan, *Cell Reports Physical Science* **1** (10) (2020) 100221.
[24] X. Li, J. Peoples, P. Yao, X. Ruan, *ACS Appl. Mater. Interfaces* **13** (18) (2021) 21733.
[25] P. Li, A. Wang, J. Fan, Q. Kang, P. Jiang, H. Bao, X. Huang, *Adv. Funct. Mater.* **32** (5) (2022) 2109542.
[26] T. Hendricks, T. Caillat, T. Mori, *Energies* **15** (19) (2022) 7307.
[27] A. P. Raman, W. Li, S. Fan, *Joule* **3** (2019) 1.
[28] E. Mu, Z. Wu, Z. Wu, X. Chen, Y. Liu, X. Fu, Z. Hu, *Nano Energy* **55** (2019) 494.
[29] Z. Zhan, M. Elkabbash, Z. Li, X. Li, J. Zhang, J. Rutledge, S. Singh, C. Guo, *Nano Energy* **65** (2019) 104060.
[30] Y. Tian, X. Liu, F. Chen, Y. Zheng, *Sci. Rep.* **10** (1) (2020) 20903.
[31] Z. Xia, Z. Zhang, Z. Meng, Z. Yu, *Journal of Quantitative Spectroscopy and Radiative Transfer* **251** (2020) 107038.
[32] S. Assawaworrarit, Z. Omair, S. Fan, *Appl. Phys. Lett.* **120** (14) (2022)
[33] A. M. Alajlan, A. A. Almethen, H. Qasem, *Appl. Phys. Lett.* **121** (7) (2022)
[34] Y. Ji, and S. Lv, *Energy* **268** (2023) 126734.
[35] Z. Xia, Z. Zhang, Z. Meng, L. Ding, Z. Yu, *ACS Appl. Mater. Interfaces* **11** (37) (2019) 33941.
[36] S. Ishii, T. D. Dao, T. Nagao, *Appl. Phys. Lett.* **117** (1) (2020) 013901.

[37] S. Khan, J. Kim, K. Roh, G. Park, W. Kim, *Nano Energy* **87** (2021) 106180.
[38] W. Ren, Y. Sun, D. Zhao, A. Aili, S. Zhang, C. Shi, J. Zhang, H. Geng, J. Zhang, L. Zhang, J. Xiao, R. Yang, *Sci. Adv.* **7** (7) (2021) eabe0586.
[39] Y. Liu, S. Hou, X. Wang, L. Yin, Z. Wu, X. Wang, J. Mao, J. Sui, X. Liu, Q. Zhang, Z. Liu, F. Cao, *Small* **18** (10) (2022) 2106875.
[40] K. Gao, J. Yang, H. Shen, Y. Liu, Y. Li, M. Zhang, *Solar RRL* **6** (2) (2022) 2100975.
[41] S. Zhang, Z. Wu, Z. Liu, E. Mu, Y. Liu, Y. Lv, T. Thundat, Z. Hu, *Adv. Mater. Technol.* **7** (12) (2022) 2200478.
[42] J. Liu, D. Li, W. Ma, Y. Chen, C. Dou, D. Meng, Q. He, X. Li, X. Deng, H. Cai, *Opt. Express* **31** (9) (2023) 14495.
[43] C.-H. Wang, H. Chen, Z.-Y. Jiang, X.-X. Zhang, *Energy* **263** (2023) 125735.
[44] M. Liao, D. Banerjee, T. Hallberg, C. Åkerlind, M. M. Alam, Q. Zhang, H. Kariis, D. Zhao, M. P. Jonsson, *Adv. Sci.* **10** (8) (2023) 2206510.
[45] S. Ishii, A. Miura, T. Nagao, K. Uchida, *Sci. Technol. Adv. Mater.* **22** (1) (2021) 441.
[46] N. P. Klochko, K. S. Klepikova, V. R. Kopach, I. I. Tyukhov, D. O. Zhadan, G. S. Khrypunov, S. I. Petrushenko, S. V. Dukarov, V. M. Lyubov, M. V. Kirichenko, A. L. Khrypunova, *Sol. Energy* **171** (2018) 704.
[47] J. Loureiro, N. Neves, R. Barros, T. Mateus, R. Santos, S. Filonovich, S. Reparaz, C. M. Sotomayor-Torres, F. Wyczisk, L. Divay, R. Martins, I. Ferreira, *J. Mater. Chem. A* **2** (18) (2014) 6649.
[48] V. Brinzari, I. Damaskin, L. Trakhtenberg, B. K. Cho, G. Korotcenkov, *Thin Solid Films* **552** (2014) 225.
[49] M. Uenuma, J. C. Felizco, D. Senaha, Y. Uraoka, *Journal of Physics: Conference Series* **1052** (1) (2018) 012011.
[50] Y. Fujimoto, M. Uenuma, Y. Ishikawa, Y. Uraoka, *AIP Adv.* **5** (9) (2015)
[51] N. Yamada, R. Ino, Y. Ninomiya, *Chem. Mater.* **28** (14) (2016) 4971.
[52] C. Yang, D. Souchay, M. Kneiß, M. Bogner, H. M. Wei, M. Lorenz, O. Oeckler, G. Benstetter, Y. Q. Fu, M. Grundmann, *Nat. Commun.* **8** (1) (2017) 16076.
[53] J. Coroa, B. M. Morais Faustino, A. Marques, C. Bianchi, T. Koskinen, T. Juntunen, I. Tittonen, I. Ferreira, *RSC Adv.* **9** (61) (2019) 35384.
[54] P. P. Murmu, V. Karthik, Z. Liu, V. Jovic, T. Mori, W. L. Yang, K. E. Smith, J. V. Kennedy, *ACS Appl. Energy Mater.* **3** (10) (2020) 10037.
[55] B. M. Morais Faustino, D. Gomes, J. Faria, T. Juntunen, G. Gaspar, C. Bianchi, A. Almeida, A. Marques, I. Tittonen, I. Ferreira, *Sci. Rep.* **8** (1) (2018) 6867.
[56] M. Uenuma, K. Umeda, J. Felizco, D. Senaha, Y. Uraoka, *J. Electron. Mater.* **48** (4) (2019) 1971.